Metals **2015**, *5*, 102-118; doi:10.3390/met5010102

OPEN ACCESS

metals

ISSN 2075-4701
www.mdpi.com/journal/metals/

Article

The Effect of Indium Content on the Atomic Environment and Cluster Stability of $GeSe_4In_{x=10,15}$ Glasses

Georgios S. E. Antipas *, Eleni Mangiorou and Evangelos Hristoforou

School of Mining Engineering and Metallurgy, National Technical University of Athens, Zografou Campus, Athens 15780, Greece; E-Mails: mangiorou.eleni@gmail.com (E.M.); eh@metal.ntua.gr (E.H.)

* Author to whom correspondence should be addressed; E-Mail: gantipas@metal.ntua.gr; Tel.: +30-210-7722037.

Academic Editor: Hugo F. Lopez

Received: 27 October 2014 / Accepted: 8 January 2015 / Published: 14 January 2015

Abstract: The atomic environments of two chalcogenide glasses, with compositions $GeSe_4In_{10}$ and $GeSe_4In_{15}$, were studied via Reverse Monte Carlo and Density Functional Theory. Indium content demoted Ge–Se bonding in favor of Se-In while the contribution of Se–Se in the first coordination shell order was faint. Upon transition to the richer In glass, there was formation of rich Ge-centered clusters at radial distances further than 4 Å from the RMC box center, which was taken to signify a reduction of Ge–Se interactions. Cluster coordination by Se promoted stability while, very conclusively, In coordination lowered cluster stability by intervening in the Ge–Se and Se–Se networks.

Keywords: Ge–Se–In glass; solute-solvent interactions; electronic structure; density functional theory

---

1. Introduction

Original interest in the Ge–Se matrix stems from its popularity in the synthesis of semiconducting materials and, in turn, investigation of electron transport in disordered Ge–Se systems is actively pursued [1,2]. The addition of a third component in Ge–Se-based glasses has raised interest regarding the system's structure [3,4] in applications such as amorphous chalcogenide membranes and ion selective

electrodes for the detection of metals in aqueous solutions [5]. Two properties regarding the amorphous Ge–Se matrix are of particular importance in applications: the material's optical band gap [1,6] (for example, Ge–Se vibrational spectroscopy [7] has revealed the instrumental role of the system's band gap on the electrical properties of Ge–Se based semiconductors) and the effect of alloying additions in the Ge–Se matrix. Typically, the introduction of Bi or Pb in a Ge–Se glass induces a change in the electrical conductivity from p- to n-type, accompanied by a reduction of the electrical resistance [8].

Indium elemental additions have been determined to affect the Ge–Se glass transition temperature (T_g) in the range of 5–8 at% In [9]. On the assumption that In atoms bond tetrahedrally, it has been shown that the Fermi energy, E_F, moves towards the valence band with increasing In content maintaining the materials p-type character [10]. Moreover, for In content up to 10 at%, the ternary material's optical band gap is unaffected while its electrical activation energy is greatly affected [10], hence the role of the solute is not settled. In ternary chalcogenide glasses for which the composition of two elements is fixed, atomic volume appears to be determined by the average coordination requirement of each species [11]. In mostly covalent glasses, the coordination number obeys the 8-N rule, where N is the valency of an atom [11]. It has previously been suggested that a stable vitreous state in chalcogenide glasses can be obtained only if enough lone-pair electrons exist in the structure of the chalcogenide system [12] and that the cation in the chalcogenide glasses may interact with the lone-pair electrons of a bridging chalcogen atom and influence the glass forming ability. Most of the charged additives introduced into chalcogenide matrices tend to occupy the lowest-energy configuration (*i.e.*, they satisfy the 8-N rule) [10] thus, they do not perturb the equilibrium between acceptor and donor defects and they do not substantially affect the material's physical properties. There are, however, cases of certain additives that adopt charged configurations and which can result in a reduction of the electronic activation energy [10].

In a previous contribution, the atomic topology of ternary Ge–Se–In glasses was determined by X-ray Diffraction (XRD), Neutron Diffraction (ND) and Extended X-ray Absorption Fine Structure (EXAFS) experiments in conjunction with Reverse Monte Carlo (RMC) fitting of the total scattering datasets [13]. The simultaneous modeling of the experimental datasets for each composition enabled the determination of partial pair distribution functions and the extraction of the local atomic order in these glasses. Here, we extend the discussion of local atomic order of the $GeSe_4In_x$ system for values of x (atomic concentrations) equal to 10 and 15; we discuss the realm of the systems' electronic structure and we provide evidence that both systems may, in fact, be characterized on the basis of discrete Ge-, Se-, and In-centered atomic clusters, selected on the basis of the variation of atomic topology in the RMC supercell.

2. Methodology

Two amorphous chalcogenide systems with nominal compositions of $GeSe_4In_{10}$ and $GeSe_4In_{15}$ were studied; both systems were originally synthesized in [13] from elemental Ge, Se and In (all elements were of 99.99% purity), by sealing the required alloy constituents in quartz ampoules under an underpressure of 10^{-3} Pa and heating the mixtures up to 1273 K under continuous vibration stirring, at a rate of 2 K/min. The samples were then quenched in a mixture of ice and water and total scattering datasets were obtained by X-Ray (XRD) and Extended X-Ray Absorption Fine Structure (EXAFS)

spectroscopy. The XRD datasets were recorded by a Ge solid-state detector at the BW5 facility in HASYLAB, DESY at incident beam energy of 100 keV with a cross section equal to 4 mm^2 and appropriate corrections (background, absorption, polarization) were imposed on the resultant data. EXAFS transmission datasets (approximately 1/e) were attained with a step size of 0.5 eV in the vicinity of the absorption edge for Ge, Se and In K-edges at the HASYLAB X beamline [13].

The materials' total structure factors, S(Q), were estimated on the basis of the experimental X-ray and neutron scattering intensities attained; The total S(Q) data were then correlated to the partial structure factors, S_{ij}(Q) via the Faber–Ziman formalism [14]. According to the formalism, the atomic weights, w_{ij}, representing the correlation between any two atomic species i and j during X-ray scattering are first defined as

$$w_{ij}(\mathrm{Q}) = (2-\delta_{ij})c_i c_j \frac{f_i(\mathrm{Q}) f_j(\mathrm{Q})}{\langle f(\mathrm{Q})\rangle^2} \tag{1}$$

where Q is the scattering wavevector, equal to $4\pi\sin(\theta)/\lambda$, θ is half of the scattering angle, λ is the radiation wavelength, δ_{ij} is the Kronecker delta function, c_i is the molar fraction of the ith element in the system and f_i is the element's form factor. The system's partial structure factors are then related to the experimentally established total S(Q) via the expression

$$S(\mathrm{Q}) = \sum_{i \le j} w_{ij}(\mathrm{Q}) S_{ij}(\mathrm{Q}) \tag{2}$$

The Faber–Ziman partial structure factors, S_{ij}(Q), are, in turn, linked to the partial pair distribution functions (PDF), $g_{ij}(r)$, through the relation

$$g_{ij}(\mathrm{r}) = 1 + \frac{1}{2\pi^2 \rho_0 r} \int_0^\infty \mathrm{Q}(S_{ij}(\mathrm{Q}) - 1)\sin(\mathrm{Qr})\mathrm{dQ} \tag{3}$$

where r is the real space (Cartesian) variable and ρ_o is the alloy's number density.

In the current work, both the total and partial PDF from the Fourier-transformed structure factors originally obtained were fitted by the RMC method via use of the molecular RMC_POT code [15]. In our simulation we retained the minimum interatomic distances (cut-offs) as established in [13]. Aside from cut-offs, partial distances of furthest approach within the first coordination shell were also defined; both cut-offs and distances of furthest approach are listed in Table 1. We note here that the exact stoichiometries of the models considered were $(Ge_{0.2}Se_{0.8})_{100-x}In_x$, where x = 10 and 15, for which $GeSe_4In_x$ is shorthand notation for the relationship between the Ge and Se species. Hence, number density and its corresponding mass density refer to the exact stoichiometries. Additionally, we note that mass density measurements for the systems at hand are scarce and the principal density estimates are based on the work by Saffarini [16,17], who also provided a phenomenological expression accounting for mass density in respect to content; that work was compiled by Kaban *et al*. [13] to derive the number densities utilized here. The RMC simulation boxes each contained 3000 atoms with a number density of 0.0328 atoms/$Å^3$ estimated on the basis of $GeSe_4In_{10}$ and 0.0335 atoms/$Å^3$ estimated on the basis of $GeSe_4In_{15}$ models.

Following RMC fitting, a number of Ge-, Se- and In-centered clusters were selected as indicative of various sites within the RMC supercell, on the basis of the radial distribution of atomic environment

statistics. In previous instances of metallic glass cluster analysis [18] we have considered the metal center coordinated solely by nearest neighbors; here we treated the more realistic case of clusters inclusive of the center's second coordination shell.

Table 1. Partial interatomic cut-offs r_{min}, as well as distances of furthest approach, r_{max}, used in this study (all distances are in Å). The first column contains the atomic pair which defines each partial. The interatomic cut-off and the distance of furthest approach are the minimum and maximum distance, respectively, which is allowed between the two closest neighbours defined by the partial.

Partial	$GeSe_4In_{10}$		$GeSe_4In_{15}$	
	r_{min}	r_{max}	r_{min}	r_{max}
Ge–Se	2.00	2.95	1.95	2.95
Se–Se	1.95	2.75	2.05	2.75
Se–In	2.30	2.90	2.30	2.90

As the clusters isolated from the RMC supercell do not, in principle, correspond to any particular level of theory, they were relaxed, keeping the atom coordinates of the second coordination shell frozen, within the premise of DFT and were further analyzed for molecular orbital interactions-induced stability. Spin unrestricted DFT relaxation was carried out in the GGA BLYP [19,20] level of theory, where single-electron wave functions were expanded into uncontracted Slater-type orbitals (STO) comprising a triple-ζ basis set with two sets of polarization functions by use of the a TZ2P basis set. Calculations were all-electron for all three of the Ge ($[Ar]3d^{10}4s^24p^2$), Se ($[Ar]3d^{10}4s^24p^4$) and In ($[Kr]4d^{10}5s^25p^1$) atomic structures, corrected for relativistic effects using the zero-order regular approximation (ZORA) [21–23]; the latter is a requirement raised by the presence of In. All DFT calculations were performed with the Amsterdam density functional (ADF) program [24].

3. Results and Discussion

3.1. Pair Distribution Functions

The fit of the RMC total and partial pair distribution functions, $g(r)$, to the experimental XRD data is shown in Figure 1 while working residuals, R_w, of the RMC goodness of fit for different partials of both systems are presented in Table 2. In both $GeSe_4In_{10}$ and $GeSe_4In_{15}$, the first coordination shell peak was at 2.4 Å and the peak extended up to 2.6 Å. It is usual for Se–Se and Ge–Se nearest neighbor distances to lie well within the first shell of interatomic interactions of complex Ge–Se–In systems, as determined by ND (Se–Se peak at 2.32 Å and Ge–Se peak at 2.36 Å, respectively) [25]. However, we noticed considerable variance in the partials that comprised the first coordination shell in respect to In content. In the case of $GeSe_4In_{10}$, primary contributions in the first shell came from Ge–Se and Se–In at almost comparable intensities, with only a faint participation of Se–Se. Interestingly, the extra In content of the $GeSe_4In_{15}$ system appeared to have substantially demoted contributions from Ge–Se in favor of Se–In, the latter shaping the shell almost exclusively. The Se–In peak has been determined by EXAFS to lie in the range 2.58–2.61 Å for widely varying Ge–Se–In formula units of glassy systems

(e.g., Ge, Se and In atom numbers in the range 5–28, 65–80 and 6–20, respectively) [26]. The role of Se–Se in the first coordination shell was faint, in similarity to $GeSe_4In_{10}$.

Table 2. Total and partial working residuals, R_w, of the RMC goodness of fit for the $GeSe_4In_{10}$ and $GeSe_4In_{15}$ systems.

	Total	Ge-Ge	Se-Se	In-In	Ge-In	Se-In
$GeSe_4In_{10}$	0.31	0.16	0.41	0.23	0.16	0.46
$GeSe_4In_{15}$	0.26	0.21	0.36	0.18	0.14	0.40

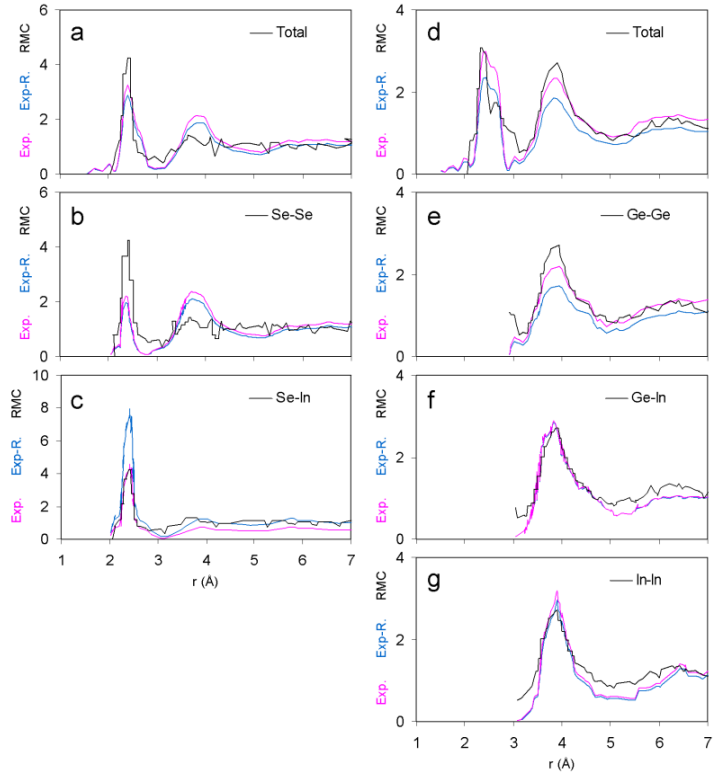

Figure 1. A comparison of RMC-derived *vs.* experimental total and partial pair distribution functions for $GeSe_4In_{10}$ (**a**–**c**) and $GeSe_4In_{15}$ (**d**–**g**). Color coding is as follows: experimental data—pink line; renormalized experimental data, blue line; and RMC, black line. Experimental data renormalization factors were: (**a**) 1.132420, (**b**) 1.122437, (**c**) 0.574149 for the $GeSe_4In_{10}$ system and (**d**) 1.266068, (**e**) 1.270162, (**f**) 1.009675 and (**g**) 1.082473 for the $GeSe_4In_{15}$ system. We note that renormalization comprised linear regression of the experimental data in the final stage of the RMC simulation towards achieving a better fit to the RMC solution.

In both systems, interactions beyond the first coordination shell revealed an almost-identical behavior of all partials involved. The peak of the total PDF second coordination shell was at 2.9 Å while the shell extended up to 3.2 Å for both systems. Here, decisive contributions towards second shell formation came from the Se-In partial with minute contributions from Ge-In and this behavior was common the two alloys. Also, third shell interatomic interactions comprised two overlapping peaks. In both alloys these peaks were at 3.3 and 3.5 Å and were owing to a combination of Se-In and In-In

interactions; the third coordination shell extended up to about 4.1 and 4.3 Å for $GeSe_4In_{10}$ and $GeSe_4In_{15}$, respectively. Longer-range order in the $GeSe_4In_{10}$ system was exclusively due to the In–In partial.

3.2. Atomic Environment Statistics and Cluster Selection

Histograms of atom coordination number, cluster number density and cluster mass density within the second coordination shell of interatomic interactions are shown in Figure 2. In the $GeSe_4In_{10}$ system, average coordination of the Ge, Se and In species was 12.51, 13.17 and 14.26, respectively. The same quantities in the $GeSe_4In_{15}$ alloy were 16.11, 14.15 and 14.20, respectively. The marked increase of Ge coordination in the $GeSe_4In_{15}$ alloy was owing to a broader and higher Ge–Se peak compared to $GeSe_4In_{10}$; hence transition to a higher In content caused an increase in Ge and Se coordination but left In coordination largely unaffected. In comparison, Ge, Se and In nearest neighbor coordination in the $GeSe_4In_{10}$ system was 3.28, 2.36, 1.07, while the same quantities for the case of the $GeSe_4In_{15}$ system were 2.04, 2.15, 1.06, respectively; as discussed in 3.1, the reduction of Ge average coordination was purely due to Se depletion in favor of bonding with In. Therefore, upon transition from $GeSe_4In_{10}$ to $GeSe_4In_{15}$, the excess In mediates more intense interaction between Se and In, a side-effect of which is Se depletion from the first coordination shell of Ge atoms. The Se species, however, remains within Germanium's second coordination shell, hence the increased average coordination of the Ge centers.

On the basis average atomic coordination, average cluster number density as well as cluster radial distribution of these quantities, we selected a number of clusters as representative of the RMC supercell; cluster radial distributions were constructed by first considering clusters centered on each of the atomic species in the RMC supercell and surrounded inclusive of second nearest neighbors. Then, the center's average and partial coordination numbers as well as the cluster's number density and average density were binned based on the center's distance from the RMC supercell center, normalized by the volume of the spherical shell corresponding to each bin. Normalization by the volume of the spherical shell intrinsically created a bias towards coordination features located close to the RMC box origin.

The radial variation of metal center coordination number and cluster number density is shown in Figure 3. In the case of the $GeSe_4In_{10}$ system, Ge-centered clusters revealed a principal tendency for 14-fold coordination (see Figure 3a) at average number density in the region of 0.03 atoms/$Å^3$ (rounded up to two decimal points—see Figure 3g). The locus of the highest concentration of such 14-fold coordinated clusters was the region up to a radial distance of 4 Å from the RMC box origin. Interestingly, there was little to no tendency for coordination of Ge centers by Ge surface atoms (see Figure 3d) mainly due to the small number of Ge atoms in the system. Se and In coordination features were interrelated and they will be discussed alongside. As seen in Figure 3b, Se principal coordination was 11 up to 4 Å from the RMC box origin. A second Se coordination feature involved 15 atoms to within 6 Å from the origin. These two features appear to loosely overlap with In coordination of 14 and as high as 17 up to 4 Å from the RMC box origin (see Figure 3c). The extent of Se–In interaction was in fact wide, as reflected in the similarity of the surfaces in Figure 3b,c, covering up to 21 Å of radial distance. Another common feature between Se- and In-centered clusters was that they both consistently involved no more than two Ge surface atoms along the whole of the RMC box radial direction (see Figure 3e,f).

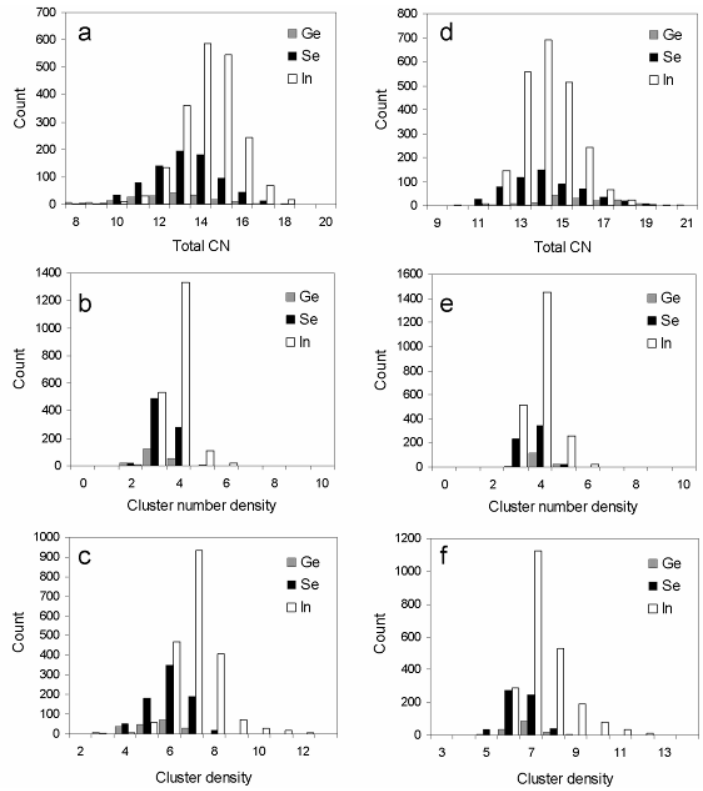

Figure 2. Particle histograms (*i.e.*, number of particles in each histogram bin *vs.* coordination number, CN, cluster number density and mass density) within the second coordination shell of interatomic interactions. Panels (**a**) to (**c**) refer to $GeSe_4In_{10}$ and panels (**d**) to (**f**) refer to $GeSe_4In_{15}$. The cluster number density values must be multiplied by 0.01 to yield units of atoms/Å^3. Cluster density is expressed in g/mL.

In the case of the $GeSe_4In_{15}$ alloy, Ge coordination in the vicinity of the RMC box origin was demoted in favor of 15-fold coordination at a radius of 8 Å, as shown in Figure 3j. One possible physical connotation attached to this transition could be the increase of coordination variability of the Ge species along the radial direction, mediated by the excess In content. The term variability is meant to denote coordination features close to the RMC box origin becoming smoother (less 'important' in radial distribution terms) with the simultaneous surfacing of features at further radial positions becoming more distinguishable (for example see features between 12 and 16 radial Å in Figure 3j). Such a transition would certainly entail breaking of Ge–Se bonds, as the prevailing partial towards Ge-induced order in the $GeSe_4In_{10}$ system was Ge–Se; correspondingly, there was reduced variability observed in Se coordination features (see Figure 3k in comparison to Figure 3b); this suggests that Se assumed specific bonding interactions, which, in fact, were in conjunction with the In species as shown by the presence of both species in features up to 4 Å of radial distance (see Figure 3k in conjunction with Figure 3l). Moreover, the coordination requirements of both Se and In for Ge surface species were reduced, in comparison to the $GeSe_4In_{10}$ system (see Figure 3n,o); inevitably, the Ge species not serving as closest neighbors of the Se and In species close to the RMC box origin, are the ones creating the coordination motifs of Figure 3j. Hence, another feature of the excess In content is the formation of rich Ge-centered clusters at radial distances further than 4 Å from the RMC center. Details of the selected clusters are listed in Table 3 while cluster geometries are shown in Figure 4.

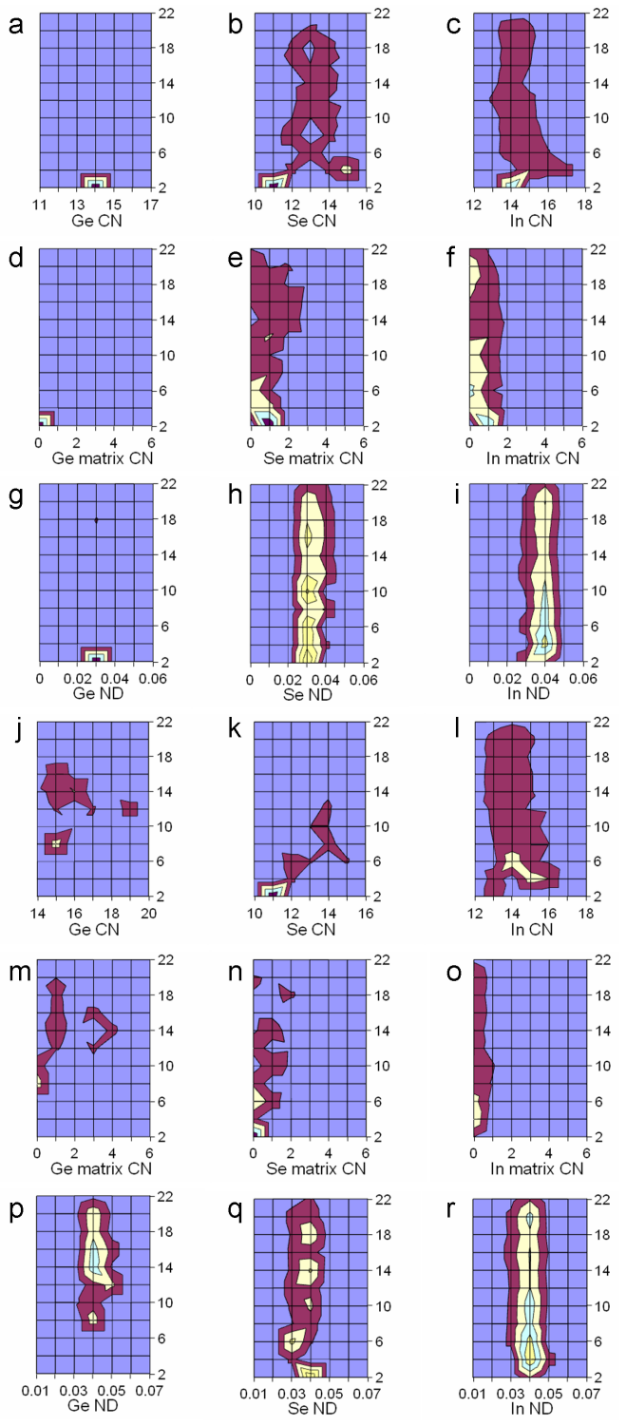

Figure 3. Surface plots of the radial distribution of coordination and number density for Ge-, Se- and In-centered clusters (the radial direction is measured from the origin of the RMC simulation box and is the vertical axis in units of Å). Panels (**a**) to (**i**) refer to the $GeSe_4In_{10}$ system while (**j**) to (**r**) refer to $GeSe_4In_{15}$. Horizontal axis notation is as follows: CN: average coordination number, matrix CN: average coordination of the cluster center by Ge ("matrix" refers to the first atomic species in the chemical formula, *i.e.*, Ge, by convention), ND: number density (atoms/$Å^3$) and D: density (g/mL). Increasing iso-surface values are shown as a progression of blue, dark red, pale white, yellow, cyan and dark brown colors.

Table 3. A list of the most characteristic clusters of the $GeSe_4In_{10}$ and $GeSe_4In_{15}$ systems selected on the basis of the radial distributions of cluster center average coordination, cluster center coordination by the matrix species (Ge) and cluster number density. In the forthcoming discussion, cluster notation will be defined by mention of the reference system first (e.g., $GeSe_4In_{10}$) followed by the center atom and the cluster designation, which is unique to the cluster (e.g., Ge_{34}, hence the cluster corresponding to the first row of this table will be $GeSe_4In_{10}$-Ge_{34}).

Reference system	Center atom	Cluster designation	Average coordination of cluster center	Cluster density (g/mL)	Cluster number density (Atoms/Å^3)	Central atom distance from RMC box origin (Å)	Number of Ge surface atoms	Number of Se surface atoms	Number of In surface atoms
$GeSe_4In_{10}$	Ge	34	14	6.268	0.03(2859)	2.865	0	2	12
$GeSe_4In_{10}$	Se	248	14	6.410	0.03(3600)	3.037	1	1	12
$GeSe_4In_{10}$	Se	371	11	5.598	0.03(0197)	2.734	1	2	8
$GeSe_4In_{10}$	In	1276	14	7.709	0.04(1329)	1.256	1	3	10
$GeSe_4In_{10}$	In	2088	15	6.716	0.03(5206)	4.513	1	2	12
$GeSe_4In_{15}$	Ge	61	16	6.995	0.03(8950)	9.441	0	5	11
$GeSe_4In_{15}$	Ge	73	15	7.224	0.03(9512)	23.148	0	4	11
$GeSe_4In_{15}$	Ge	109	15	7.053	0.03(6971)	23.075	0	2	13
$GeSe_4In_{15}$	Se	479	12	6.779	0.03(4477)	6.715	0	1	11
$GeSe_4In_{15}$	Se	564	14	6.765	0.03(4554)	8.228	0	1	13
$GeSe_4In_{15}$	Se	668	11	7.518	0.03(7109)	2.086	0	0	11
$GeSe_4In_{15}$	Se	671	14	7.713	0.04(1187)	8.277	0	3	11
$GeSe_4In_{15}$	Se	713	13	5.878	0.03(0678)	5.771	0	2	11
$GeSe_4In_{15}$	In	865	14	7.563	0.03(9488)	6.124	0	3	11
$GeSe_4In_{15}$	In	1735	14	6.772	0.03(3854)	5.810	0	1	13
$GeSe_4In_{15}$	In	2219	14	7.458	0.03(9824)	5.467	0	4	10
$GeSe_4In_{15}$	In	2502	17	7.582	0.04(0358)	6.267	0	4	13

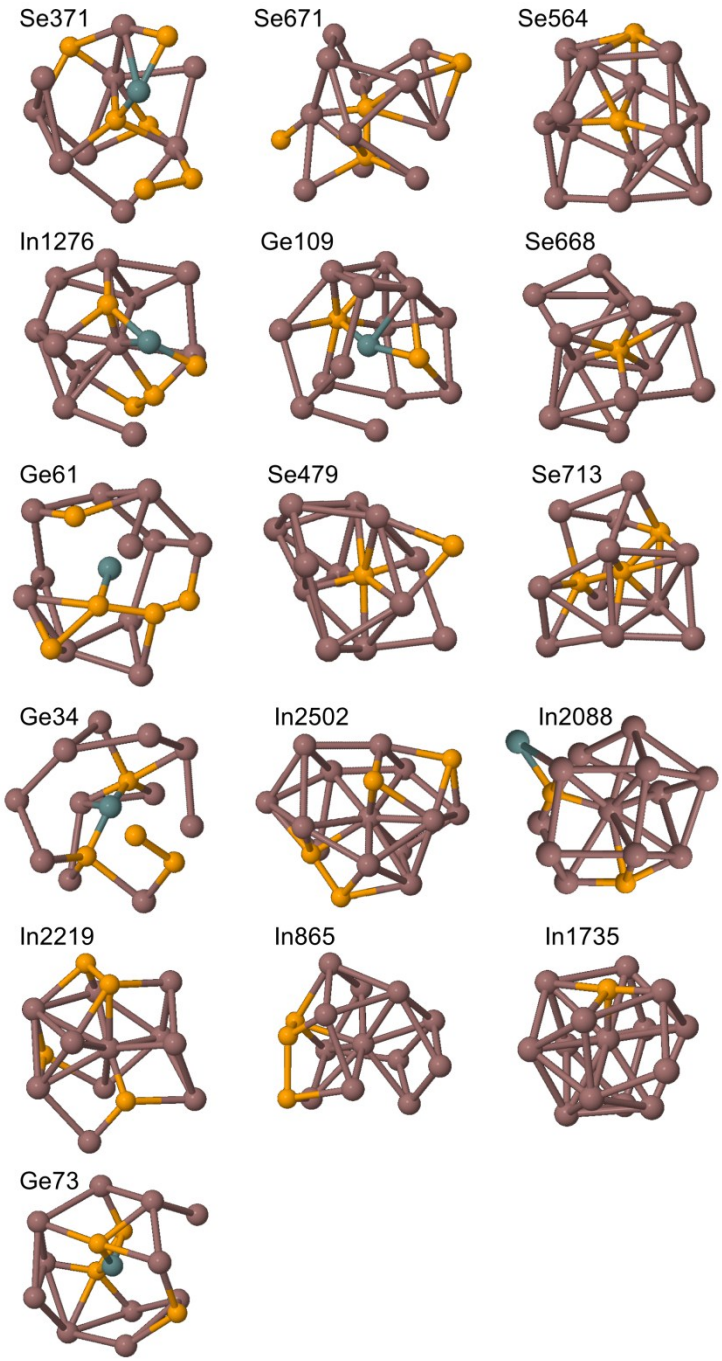

Figure 4. Geometries of the most representative clusters as isolated from the RMC supercell. Cluster designations refer to Table 3. Color coding is as follows: In, dark purple; Se, orange; and Ge, dark blue.

3.3. Binding Energy Decomposition and Molecular Orbital Interactions

In our previous study of covalent glasses, it was shown that the ground state of isolated metallic clusters was best described by negatively charged moieties [18] of rather high spin multiplicities (typically up to 12). Cluster relaxation was as a matter of principle not possible under charge neutrality, and it, thus, required charge compensations accompanied by spin polarization. In the current study we have required that all clusters be charge-neutral, spin-unpolarized moieties if possible, while we have considered the lowest spin multiplets for clusters for which charge neutrality demanded spin

compensation. As it turned out, the majority of the clusters considered did, in fact, relax at lower energy states under the effect of spin polarization. Cluster spin polarization and binding energy decomposition is listed in Table 4 and the decomposition of cluster binding energy into its constituent Pauli, electrostatic and orbital interaction energies is presented in Figure 5. The principal feature of cluster stability was the extent of orbital interactions energy. Secondarily, the difference between orbital interactions and Pauli repulsion could also be correlated to cluster stability. Invariably, electrostatic interactions were not deemed to be monotonically related to the stability of the complexes studied.

Table 4. Spin polarization, number of electrons, N_e, and binding energy decomposition for the clusters studied.

Cluster name	Spin polarization	N_e	Pauli (a.u.)	Electrostatic (a.u.)	Orbital Interactions (a.u.)
$GeSe_4In_{10}$-Se_{371}	1	526	5.201	−1.666	−4.925
$GeSe_4In_{10}$-In_{1276}	1	673	6.341	−2.053	−5.522
$GeSe_4In_{15}$-Ge_{61}	1	741	6.011	−1.966	−5.379
$GeSe_4In_{10}$-Ge_{34}	1	688	4.781	−1.545	−4.439
$GeSe_4In_{15}$-In_{2219}	1	675	5.701	−1.823	−5.046
$GeSe_4In_{15}$-Ge_{73}	1	707	6.151	−2.035	−5.304
$GeSe_4In_{15}$-Se_{671}	1	675	5.269	−1.721	−4.671
$GeSe_4In_{15}$-Ge_{109}	1	737	4.701	−1.401	−4.491
$GeSe_4In_{15}$-Se_{479}	0	607	4.729	−1.465	−4.231
$GeSe_4In_{15}$-In_{2502}	1	822	6.708	−2.134	−5.866
$GeSe_4In_{15}$-In_{865}	0	690	5.335	−1.673	−4.737
$GeSe_4In_{15}$-Se_{564}	1	705	5.040	−1.528	−4.586
$GeSe_4In_{15}$-Se_{668}	0	573	3.983	−1.207	−3.626
$GeSe_4In_{15}$-Se_{713}	1	641	5.860	−1.955	−4.839
$GeSe_4In_{10}$-In_{2088}	0	737	6.065	−1.924	−5.166
$GeSe_4In_{15}$-In_{1735}	0	720	5.094	−1.535	−4.551
$GeSe_4In_{10}$-Se_{248}	1	688	4.032	−1.301	−3.576

A rather more concrete measure of cluster stability, however, was highlighted by cluster center coordination. Cluster binding energy in respect to the center's Se and In coordination numbers is shown in Figure 6, where coordination by Ge atoms was not included as Ge content was too low to provide meaningful statistics. Based on the trends shown in Figure 6, it became clear that cluster stability (regardless of the position and the species type of cluster center) was fundamentally correlated to coordination by Se. As laid out in 3.1, order within the first coordination shell involved the Ge–Se and Se–In partials while the effect of In came into effect beyond the first shell. Therefore, we deem that Ge–Se and Se–In bonding promotes cluster stability and, correspondingly, the intervention of the In species which caused breaking of these bonds contributed towards a lower binding energy, also as shown in Figure 5.

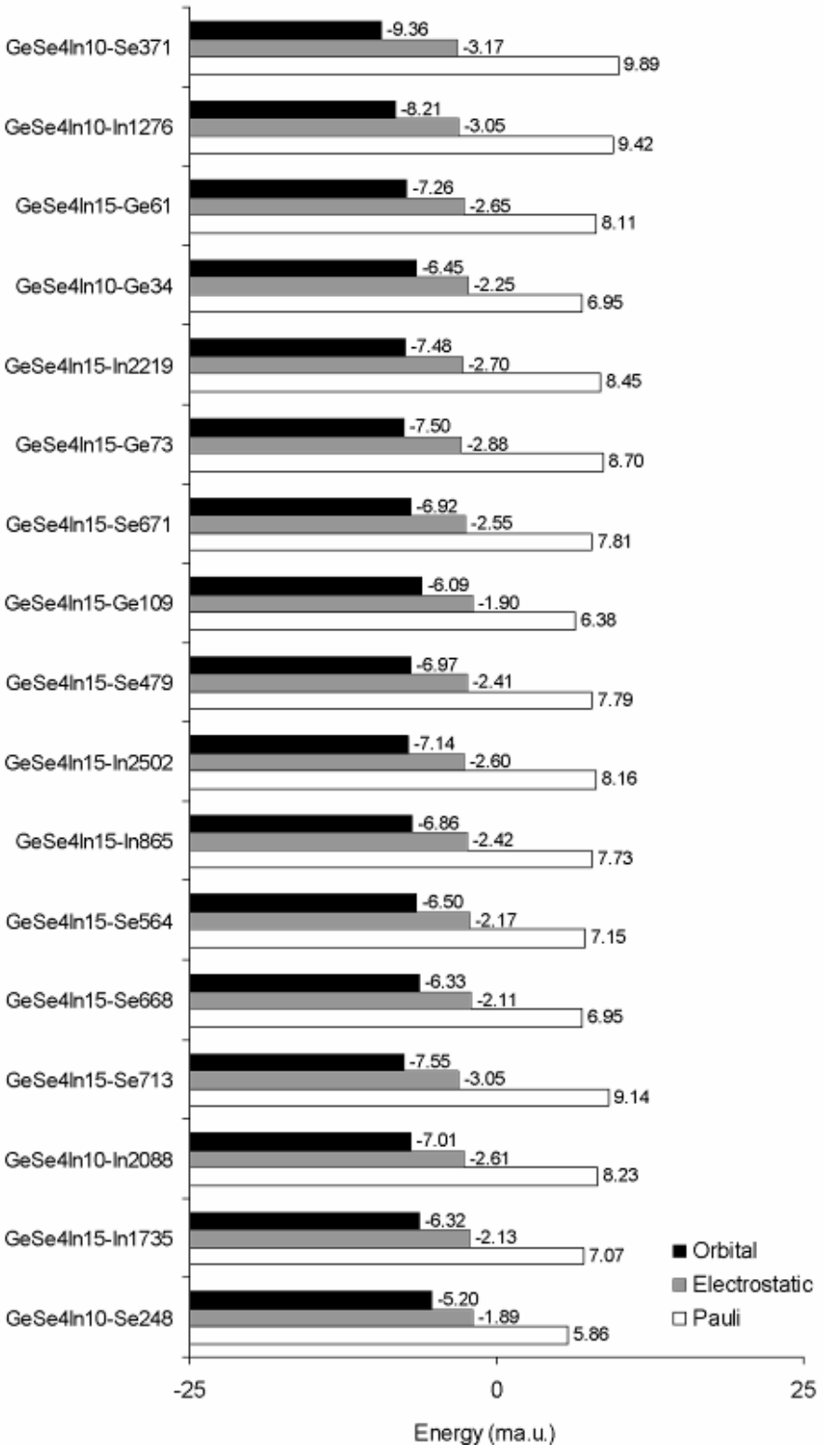

Figure 5. Binding energy decomposition of the most representative clusters for both systems under study. From top to bottom, cluster energy is in ascending energy order (thus, clusters $GeSe_4In_{10}$-Se_{371} and $GeSe_4In_{10}$-Se_{248} are the most cohesive and least cohesive, respectively).

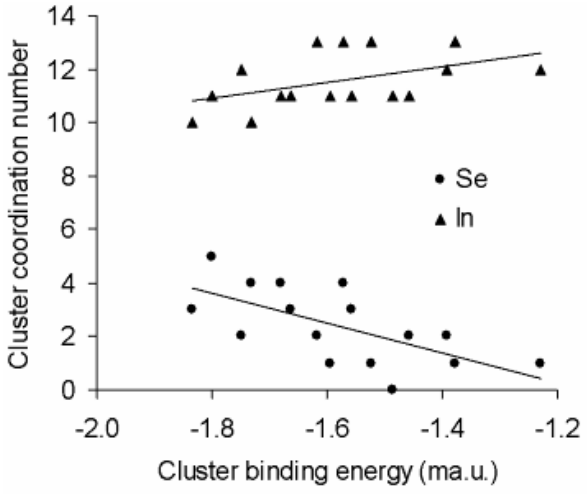

Figure 6. Cluster binding energy, normalized by the number of electrons in each cluster, in respect to the center's partial coordination numbers by the Se and In species. Ge content was always too low to provide a meaningful trend on the same plot.

Atomic orbital t_{1u} contributions for the most representative clusters under study are shown in Figure 7, as percentages of total molecular orbital density. There was no monotonic relationship between cluster binding energy and the contribution of atomic orbitals. At first glance, the participation of Ge in MO's is not symptomatic to the system and in extension it is neither symptomatic to In content. Also, Ge contributions were not particular to the cluster center's average coordination. However, in the $GeSe_4In_{10}$ system, Ge contributed towards higher lying MO's while this was not the case in $GeSe_4In_{15}$. All high lying MO's of the latter system either involved pure In contributions (e.g., see clusters Se_{668} and In_{1735} in Figure 7) or fractional valence contributions from Se mixed with major contributions from In (see clusters In_{2219}, Se_{671}, Se_{479}, In_{2502}, In_{865} and Se_{564} and Se_{713} in Figure 7). The competition between Ge and In conforms to a previously established observation that at high effective In concentrations, In atoms tend to engage Ge atoms by entering into $GeSe_{4/2}$ tetrahedra and adopting Ge–In bonds [10]. However, the landmark feature of both systems was the cooperation between Se and In. We consider this to be reminiscent of In_2Se_3 structural units, as these have been frequently mentioned as responsible for short-range ordering in a wide range of glasses [26]. Gradual addition of Indium to these glasses has been reported as responsible for the replacement of stronger Ge–Se bonds by weaker Ge–Ge interactions towards formation of In_2Se_3 units [10] or towards the substitution of lone Se atoms in $(Se)_n$ chains [2]. As we have already reported in [27], Indium saturation of Se bonds is more effective at high In/Se ratios. At lower ratios, such as the $GeSe_4In_{10}$ system, the effect of Ge–Se cooperation is swift to set back in and a depiction of this is provided in Figure 6 by the $GeSe_4In_{10}$ clusters. This trend is also on a par with observations that increasing Ge/Se ratios caused the replacement of Se–Se and Se–In bonds by Ge–Ge, Ge–Se and Ge–In bonds [28] while increasing In content saturates Se–In bonds at the expense of Ge [6].

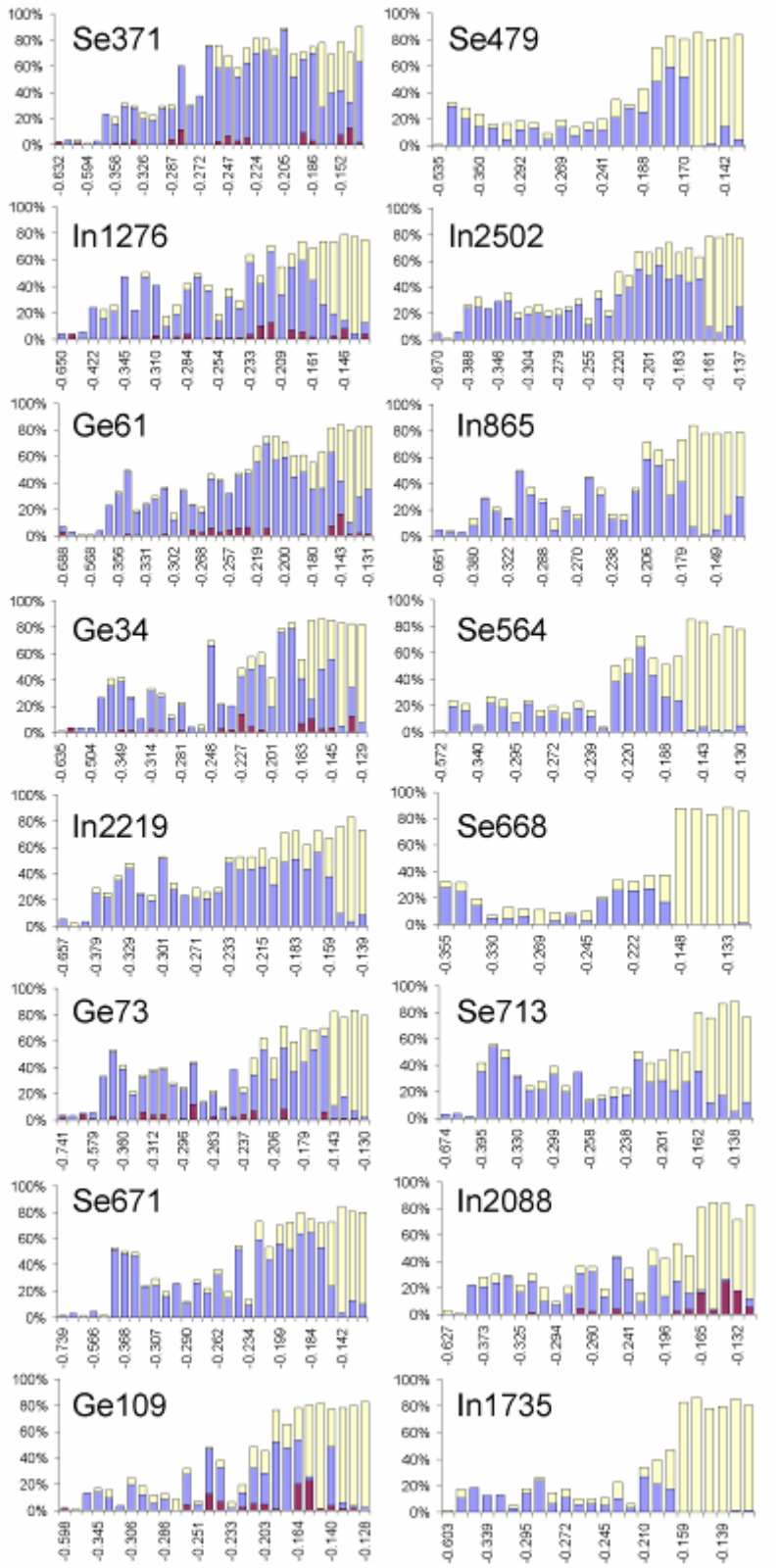

Figure 7. Atomic orbital t_{1u} contributions as a percentage of total molecular orbital density for the most representative clusters under study. Color notation is as follows: Ge, dark red; Se, light blue; and In, light yellow.

4. Conclusions

The combined analysis of RMC atomic environment statistics and DFT study of a number of representative clusters of the $GeSe_4In_{10}$ and $GeSe_4In_{15}$ glasses allowed the following conclusions to be drawn:

(1) The extra In content of the $GeSe_4In_{15}$ system appeared to have substantially demoted contributions from Ge–Se in favor of Se–In, which shaped the shell almost exclusively. The role of Se–Se was faint, in similarity to $GeSe_4In_{10}$.
(2) In both glasses studied, interactions beyond the first coordination shell revealed great similarity among the shapes of the partials involved. The Se–In partial was instrumental towards second coordination shell formation; Ge–In contributed only fractionally towards second coordination and this behavior was common to both alloys. Third shell interatomic interactions comprised two overlapping peaks at 3.3 and 3.5 Å due to Se–In and In–In interactions.
(3) The excess In content in $GeSe_4In_{15}$ mediated the formation of rich Ge-centered clusters at radial distances further than 4 Å from the RMC center, an effect which also flagged the reduction of bonding between Ge and Se near the RMC center.
(4) Ge–Se and Se–In bonding promoted overall cluster stability and the intervention of excess In caused breaking of these bonds contributed towards a lower binding energy.
(5) The introduction of excess In resulted in higher Se–In cooperation towards frontier orbitals. Direct interactions between Ge and In were scarce and limited to the $GeSe_4In_{10}$ glass. On the whole, Ge and Se competed for connectivity with Se over the whole range of valence electron energies; however, Indium, particularly in the $GeSe_4In_{15}$ system, was far more effective in bonding with Se.

Author Contributions

EH and GA designed the analysis methodology, interpreted the results and wrote the paper. EM and GA performed the analysis. All authors discussed on the paper throughout all of the stages.

Conflicts of Interest

The authors declare no conflict of interest.

References

1. Saffarini, G.; Saiter, J.M.; Schmitt, H. The composition dependence of the optical band gap in Ge–Se–In thin films. *Opt. Mater.* **2007**, *29*, 1143–1147.
2. Kumar, A.; Husain, M.; Swarup, S.; Nigam, A.N.; Kumar, A. X-ray spectroscopic studies in glassy semiconducting $Ge_{20}Se_{80}$ and $Ge_{20}Se_{80-x}In_x$ alloys. *Physica B* **1990**, *162*, 177–180.
3. Dejus, R.J.; Susman, S.; Volin, K.J.; Montague, D.G.; Price, D.L. Structure of vitreous AgGeSe. *J. Non-Cryst. Solids* **1992**, *143*, 162–180.
4. Usuki, T.; Uemura, O.; Fujimura, K.; Kameda, Y. Local arrangement in Ge-Se-In glasses. *J. Non-Cryst. Solids* **1995**, *192–193*, 69–73.

5. Conde Garrido, J.M.; Ureña, M.A.; Arcondo, B. Ion selective electrodes based on chalcogenide glasses. *J. Alloys Compd.* **2010**, *495*, 356–359.
6. Sharma, I.; Tripathi, S.K.; Monga, A.; Barman, P.B. Electrical properties of a-Ge-Se-In thin films. *J. Non-Cryst. Solids* **2008**, *354*, 3215–3219.
7. Goyal, D.R.; Maan, A.S. Far-infrared absorption in amorphous $Sb_{15}Ge_xSe_{85-x}$ glasses. *J. Non-Cryst. Solids* **1995**, *183*, 182–185.
8. Tohge, N.; Minami, T.; Yamamoto, Y.; Tanaka, M. Electrical and optical properties of n-type semiconducting chalcogenide glasses in the system Ge-Bi-Se. *J. Appl. Phys.* **1980**, *51*, 1048–1053.
9. Giridhar, A.; Mahadevan, S. The T_g *versus* Z dependence of glasses of the Ge-In-Se system. *J. Non-Cryst. Solids* **1992**, *151*, 245–252.
10. Rabinal, M.K.; Sangunni, K.S.; Gopal, E.S.R. Chemical ordering in $Ge_{20}Se_{80-x}In_x$ glasses. *J. Non-Cryst. Solids* **1995**, *188*, 98–106.
11. Tanaka, K. Structural phase transitions in chalcogenide glasses. *Phys. Review B* **1989**, *39*, 1270–1279.
12. Liang, Z. Chemical bond approach to the chalcogenide glass forming tendency. *J. Non-Cryst. Solids* **1991**, *127*, 298–305.
13. Kaban, I.; Jovari, P.; Petkova, T.; Petkov, P.; Stoilova, A.; Hoyer, W.; Beuneu, B. Structure of $GeSe_4$-In and $GeSe_5$-In glasses. *J. Phys*. *Condens. Matter* **2010**, *22*, 404205.
14. Faber, T.E.; Ziman, J.M. A theory of the electrical properties of liquid metals. *Philos. Mag.* **1965**, *11*, 153–173.
15. Gereben, O.; Pusztai, L. RMC_POT: A computer code for reverse Monte Carlo modeling the structure of disordered systems containing molecules of arbitrary complexity. *J. Comput. Chem.* **2012**, *33*, 2285–2291.
16. Saffarini, G. Fragmentation of $Ge_{1-x}Sn_xSe_2$ glasses. *Solid State Commun.* **1994**, *10*, 677–681.
17. Saffarini, G. Atomic density versus average coordination number in Ge–In–Se glasses. *Phys. Status Solidi* **1999**, *2*, 261–265.
18. Antipas, G.S.E. Molecular orbital interactions in glass-forming $Zr_{70}Cu_{30}$ liquid quasicrystals. *J. Alloys Compd.* **2013**, *578*, 565–570.
19. Becke, A.D. Density-functional exchange-energy approximation with correct asymptotic behavior. *Phys. Rev. A* **1988**, *38*, 3098–3100.
20. Lee, C.; Yang, W.; Parr, R.G. Development of the Colle-Salvetti correlation-energy formula into a functional of the electron density. *Phys. Rev. B* **1988**, *37*, 785–789.
21. Van Lenthe, E.; Baerends, E.J.; Snijders, J.G. Relativistic total energy using regular approximations. *J. Chem. Phys.* **1994**, *101*, 9783–9792.
22. Belanzoni, P.; van Lenthe, E.; Baerends, E.J. An evaluation of the density functional approach in the zero order regular approximation for relativistic effects: Magnetic interactions in small metal compounds. *J. Chem. Phys.* **2001**, *114*, 4421–4433.
23. Van Lenthe, E.; van der Avoird, A.; Wormer, P.E.S. Density functional calculations of molecular hyperfine interactions in the zero order regular approximation for relativistic effects. *J. Chem. Phys.* **1998**, *108*, 4783–4796.
24. *Amsterdam Density Functional Program*; Vrije Universiteit: Amsterdam, The Netherlands, 2010.

25. Salmon, P.S. Structure of liquids and glasses in the Ge–Se binary system. *J. Non-Cryst. Solids* **2007**, *353*, 2959–2974.
26. Ledru, J.; Saiter, J.M.; Saffarini, G.; Benazeth, S. An EXAFS investigation of the local order around indium in Ge–Se–In glasses. *J. Non-Cryst. Solids* **1998**, *232–234*, 634–637.
27. Antipas, G.S.E.; Mangiorou, E.; Hristoforou, E. Solute-solvent interactions and atomic cohesion in $GeSe_4$ and $GeSe_4In_5$ metallic glasses. *Mater. Res. Express* **2014**, *1*, 015202.
28. Abdel-Rahim, M.A.; Hafiz, M.M.; El-Nahass, M.M.; Shamekh, A.M. Influence of composition on optical and electrical properties of Ge–Se–In thin films. *Physica B* **2007**, *387*, 383–391.